

---

# Multi-objective Optimization of Activity-Travel Policies for Epidemic Control: Balancing Health and Economic Outcomes on Socio-Economic Segments

Cloe Cortes Balcells \*      Rico Krueger †      Michel Bierlaire \*

February 2, 2024

Report TRANSP-OR 221123  
Transport and Mobility Laboratory  
School of Architecture, Civil and Environmental Engineering  
Ecole Polytechnique Fédérale de Lausanne  
[transp-or.epfl.ch](http://transp-or.epfl.ch)

---

\*École Polytechnique Fédérale de Lausanne (EPFL), School of Architecture, Civil and Environmental Engineering (ENAC), Transport and Mobility Laboratory, Switzerland, {cloe.cortes, michel.bierlaire}@epfl.ch

†Department of Technology, Management and Economics, Technical University of Denmark (DTU), {rickr@dtu.dk}

## Abstract

The COVID-19 pandemic has highlighted the importance of effective epidemic management, which depends on policies that consider the complexities of how people move and interact. This study introduces a novel decision support tool that integrates an activity-based model for mobility dynamics with a SIRD model for infection transmission. The tool consists in a multi-objective optimization framework that evaluates the trade-offs between public health and economic factors across socio-economic segments. Our findings show that policies targeted at specific demographic groups significantly improve the efficacy of interventions. The proposed framework offers policy makers a multi-objective-model approach, we can offer policymakers a set of optimized, segmented strategies, presented through an intuitive dashboard. This visualization compares potential outcomes along the Pareto frontier, helping select balanced and effective policies. The proposed model offers a significant step forward in epidemic management, providing a robust platform for data-driven decision making in crisis scenarios.

**Keywords:** activity-based modeling, SIRD model, policy optimization, epidemic management, multi-objective optimization, decision support tool.

## 1 Introduction

The global outbreak of the COVID-19 pandemic has highlighted the critical role of activity-travel behavior in understanding disease transmission dynamics, informing policy decisions and effectively managing the spread of infectious diseases. The interaction of activity-travel behavior with disease transmission indicates the need for collaboration between epidemiological and transportation communities to develop robust and efficient decision support tools (Qian and Ukkusuri, 2021; Nguyen et al., 2022; Molloy et al., 2021). Specifically, the COVID-19 pandemic has disrupted travel behavior patterns across various socio-economic segments (SES) (Xi et al., 2023), leading to substantial negative impacts on social equity (Chang et al., 2021). As we strive to understand how best to manage the spread of a disease and its repercussions, it is crucial to understand and account for the differences in activity-travel behavior between population segments and design policies that account for these variations.

As part of the effort to manage disease spread, activity-travel restrictions have been widely used to prevent hospital overload and epidemic rebound. Although some restrictions on activity travel have a significant economic and social impact on the country (Queiroz et al., 2022), resulting in substantial human and economic

loss, others manage to effectively prevent disease transmission with only minimal inconveniences and negligible impact on these areas. Therefore, it is crucial to make a clear distinction between different types of policy. Evaluating the trade-off between the health benefits and economic costs of these policies becomes crucial in guiding policy decisions during a pandemic. Although some studies in the literature take into account activity-travel behavior (Filho et al., 2022; Kerr et al., 2020; Tirachini and Cats, 2020) for disease spreading, they do not adequately integrate it into policies that effectively benefit from the fact that such behaviors vary between different population segments. Recognizing and leveraging these behavioral differences is essential to formulating segment-specific policies that provide a more effective containment in disease spreading.

To address these literature gaps, this paper aims to explore the integration of epidemiological and transportation perspectives for informed decision support in managing disease transmission for future pandemics in order to find targeted policies. For this reason, we integrate two submodels: i) an activity-based model to capture activity-travel behavior, ii) and an epidemiological model to study the spread of the disease, encapsulated by a multi-objective optimization tool that provides a set of optimal policies for each segment of the population (Pareto front). This approach allows policymakers to make informed decisions that balance public health and economic impact, targeting different socio-economic groups. We show that segment-specific policies are more effective than generalized ones, providing a more flexible response to an epidemiological crisis. The decision variable in our approach is represented as a high-dimensional tensor, which provides a method to efficiently handle the complexity involved in segment-specific policy-making, and when the policy is applied. By bridging the gap between the epidemiological and transportation communities, we can better develop robust decision-support tools that address the challenges posed by disease spread. Our approach achieves its purpose by addressing activity-travel behavior and customizing policies for different population segments, showing that one-size-fits-all policies often fail to account for the unique needs and behaviors of different demographic groups.

We organize the remainder of this paper as follows. In Section 2, we review the related literature. In Section 3, we present the methodology of our tool. In Section 4, we present the results of our case study. Finally, we conclude in Section 5.

## **2 Literature review**

In recent years, especially with the onset of COVID-19, there has been a notable shift in the epidemiological world, with the transportation community making

significant contributions. However, a common trend in this line of research is a stronger focus on the modeling aspect, often at the expense of detailed policy implementation, which is crucial for effective disease management.

Traditional epidemiological models have been criticized for their lack of heterogeneity and integration of mobility. Recognizing this gap, recent studies have begun to incorporate mobility data to improve predictions and evaluate mobility limitation strategies.

Table 1 provides a comprehensive summary of these studies, showcasing their characteristics in terms of mobility and epidemiological models, heterogeneity considerations, policy evaluations, and the types and levels of policies examined. This summary helps to contextualize our current understanding and highlights areas where further development is needed.

## **2.1 Disaggregated policies**

In the field of pandemic management, particularly in the context of COVID-19, research that focuses on disaggregated policy approaches is notably limited, to the best of the authors' knowledge. A prominent example is the study by Acemoglu et al., 2020, which stands out for its targeted approach in a multigroup SIR model, focusing on different age groups and their respective risk profiles. This study found that targeting risk/age groups with differential lockdowns significantly outperforms uniform policies. Although these policies effectively minimize both economic losses and deaths by implementing stricter lockdowns for the most vulnerable group, they are not widely explored in the literature.

Approaches that consider disaggregated policies (Acemoglu et al., 2020; Brotherhood et al., 2020), originate primarily from the epidemiological community, missing the integration of critical mobility aspects, which are crucial in the management of disease control. The lack of a comprehensive analysis of activity restrictions in these studies represents a significant gap. Bridging the epidemiological and transportation communities could provide greater insight into how, where, and between whom the disease spreads. This integration is essential for developing targeted interventions that consider not only epidemiological factors such as vaccination or confinement policies but also the dynamics of mobility and activity restrictions, crucial for a more effective response to pandemic management.

### **2.1.1 Studies focusing on mobility without comprehensive epidemiological integration**

While several studies have incorporated mobility data, a critical limitation lies in their failure to fully integrate this heterogeneity into epidemiological models. This results in a gap where the socioeconomic aspects that influence mobility are not reflected in the dynamics of disease transmission. For example, Qian and Ukkusuri, 2021 explore the impacts of mobility on disease spread, but does not explore how socioeconomic factors influencing mobility patterns are integrated into epidemiological aspects, leaving a crucial aspect of behavioral heterogeneity unaddressed. Similarly to Qian and Ukkusuri, 2021, Chang et al., 2021 focus on the general impacts of mobility but do not extend their analysis to incorporate these mobility patterns into a more heterogeneous epidemiological model. This lack of integration limits the potential for more interpretability in disease transmission and control models.

### **2.1.2 Studies bridging mobility with policy frameworks**

Some studies have attempted to bridge mobility data with policy frameworks, but with varying degrees of integration. A systematic review of COVID-19 transport policies can be found in Calderon Peralvo et al., 2022. Regarding research adopting a multi-objective perspective, we find that Yaesoubi et al., 2021 introduce a multi-objective optimization tool for physical distancing interventions, aiming to balance COVID-19 control with economic costs. This study represents an attempt to link mobility restrictions with epidemiological results, although the integration of heterogeneity into the epidemiological model could be improved by integrating individual-level probabilities of infection into the epidemiological model, rather than using a grouped approach by segment. Chen et al., 2022 develop a linear programming framework to study the trade-off between fatality rates and community reopening. Although acknowledging the multi-objective nature of the problem, the study primarily focuses on a singular intervention plan, potentially simplifying complex socioeconomic dynamics. Filho et al., 2022 use an age-structured model to optimize the vaccination strategy, but does not include a mobility model to fully capture the interaction between mobility patterns, socioeconomic factors, and epidemiological outcomes.

These studies indicate a growing recognition of the importance of integrating mobility and socio-economic factors into epidemiological models. However, there is still room for improvement, particularly in developing models that reflect the complexity of human behavior more accurately, a crucial aspect for transportation behavioral experts. This shortcoming is particularly evident in the context of

disaggregated policy approaches, where the potential for targeted interventions based on intricate mobility patterns is vast but remains unexplored.

## 2.2 Bridging the gaps with a comprehensive framework

Our study builds on the foundational work in disaggregated policy approaches, notably Acemoglu et al. (2020). We extend their work by integrating detailed analyses of mobility aspects and activity restrictions, which are key to effective pandemic management. Our approach goes beyond the current targeted policies by incorporating these critical elements into our epidemiological models. Our methodology adopts a multi-objective optimization framework, which avoids the common oversimplification of having one combined objective function. This allows for a more sophisticated analysis that considers the trade-off between public health and economic impact, allowing policymakers to decide where to draw the line in ethical implications. The high-dimensional tensor used as decision variable efficiently addresses the complexities involved in crafting segment-specific policies, facilitating a more adaptable and efficient response to epidemiological crises.

In summary, our study contributes to the relatively unexplored area of disaggregated policy approaches in pandemic management. By combining this approach with detailed analyses of mobility and activity restriction policies, we provide a more comprehensive and effective framework for pandemic management. This advance is crucial for future public health crises and disease spread management, setting a new precedent for targeted and effective pandemic response strategies.

## 3 Methodology

The model captures the dynamic of two phenomena: mobility and infection. Figure 1 shows graphically a sketch of the proposed framework. The dynamic of mobility is captured within a day, discretized into  $T$  time intervals. For each day, we consider a discretized time horizon into  $T$  time intervals of the same length. A typical discretization is 30 minutes, so the time is indexed by  $t = 1, \dots, T = 48$ . It is assumed that the mobility patterns are identical from day to day. The infection dynamic is captured in  $L$  consecutive periods, typically a day, numbered 1 to  $L$ . In the rest of the paper, we use the word “day” to refer to these periods.

The space is represented by a discrete set  $\mathcal{F}$  locations, or facilities, corresponding to the points of the perimeter that we are interested in (a city, a region, etc.) We also consider a discrete list of  $A$  activities that individuals can perform

Reference	Title	Mobility		Epidemiological			Y/N?	Multi objectives	Policy		Aggregation
		Model	Heterogeneity	Model	Type	Heterogeneity			Type		
Acemoglu et al., 2020	Optimal Targeted Lockdowns in a Multi-Group SIR Model	No		✓	Compartmental, SIR	✓	✓	No	Targeted Group Testing, Lockdowns, Distancing,	Disaggregated	
Brotherhood et al., 2020	An Economic Model of the COVID-19 Epidemic: The Importance of Testing and Age-Specific Policies	No		✓	Agent-based	✓	No	No	Testing, Confinements	Disaggregated	
Chang et al., 2021	Mobility network models of COVID-19 explain inequities and inform reopening	✓	✓	✓	Agent-based, SEIR	No	✓				
Chari et al., 2020	The Hammer and the Scalpel: On the Economics of Indiscriminate versus Targeted Isolation Policies during Pandemics	No		✓	Compartmental, SIR	✓	✓	No	Testing, Isolation	Aggregated	
Chen et al., 2022	An Optimization Framework to Study the Balance Between Expected Fatalities Due to COVID-19 and the Reopening of U.S. Communities	No		✓	Network, CC19LP	✓	✓	✓	Activity Restriction	Aggregated	
Colas et al., 2021	EpidemiOptim: A Toolbox for the Optimization of Control Policies in Epidemiological Models	No	No	✓	Agent-based, SEIR	✓	✓	✓	Quarantine	Aggregated	
Eubank et al., 2004	Modelling disease outbreaks in realistic urban social networks	✓	✓	✓	Compartmental SEIR	No	No				
Filho et al., 2022	Optimization of COVID-19 vaccination and the role of individuals with a high number of contacts: A model based approach	✓	✓	✓	Compartmental, SEIAHRV	✓	✓	No	Vaccination	Aggregated	
Ghamizi et al., 2020	Simulation and Optimization for Covid-19 Exit Strategies	✓	No	✓	Compartmental, SEIHDR	No	✓	No	Quarantine, activity-restrictions	Aggregated	
Janko et al., 2023	Optimizing non-pharmaceutical intervention strategies against COVID-19 using artificial intelligence	No	No	✓	Compartmental, SEIRD + Machine learning	No	✓	✓	Non-Pharmaceutical Interventions	Aggregated	
Kerr et al., 2020	Covasim: an agent-based model of COVID-19 dynamics and interventions	✓	✓	✓	Agent-based, SE <sup>1</sup> IRD	✓	No				
Muller et al., 2020	Using mobile phone data for epidemiological simulations of lockdowns: government interventions, behavioral changes, and resulting changes of reinfections	✓	✓	✓	Agent-based, SEIR	No	No				
Qian and Ukkusuri, 2021	Connecting urban transportation systems with the spread of infectious diseases: A Trans-SEIR modeling approach	✓	✓	✓	Compartmental, SEIR	No	No				
Yaesoubi et al., 2021	Adaptive Policies to Balance Health Benefits and Economic Costs of Physical Distancing Interventions during the COVID-19 Pandemic	No		✓	Compartmental, SEIRH	No	✓	✓	Physical distancing	Aggregated	
Our approach	Multi-objective Optimization of Activity-Travel Policies for Epidemic Control: Balancing Health and Economic Outcomes on Socio-Economic Segments	✓	✓	✓	Compartmental, Age-stratified SIRD	✓	✓	✓	Activity-restrictions	Disaggregated	

Table 1: Summary of Papers and Their Characteristics

during the day. Each activity  $\alpha$  is associated with a set of locations or facilities  $\mathcal{F}_\alpha$ .

The population is segmented into  $G$  groups, characterized by their socio-economic characteristics (age, gender, residence location). The assumption is that each group is homogeneous in terms of spread of the disease. In particular, for each group  $g$ , we assume a recovery rate  $\gamma_g$  ( $0 < \gamma_g \leq 1$ ), and a death rate  $\mu_g$ .  $\gamma_g$  is the percentage of individuals in group  $g$  who recover from the disease in a day, and  $\mu_g$  ( $0 < \mu_g \leq 1$ ), is the percentage of infected individuals in group  $g$  who die in a day, as derived from previous studies (Kerr et al., 2020).

### 3.1 Input

As input, we obtain a description of the mobility of the population from the output of a microscopic activity-based model, such as MATSim or TASHA (Horl and Balac, 2021; Yasmin et al., 2015), which generates a list of activity schedules for  $N$  individuals at day 0. Each individual  $n$  is associated with a facility  $f_{nt}$  for each time interval  $t$ , and the group  $g_n$  to which they belong. These models are suitable for simulating the travel behavior of individuals, providing the granular data necessary for our analysis. The inputs and outputs required from these types of model are found in Figure 1, which shows the integration of travel behavior data into our multi-objective optimization framework.

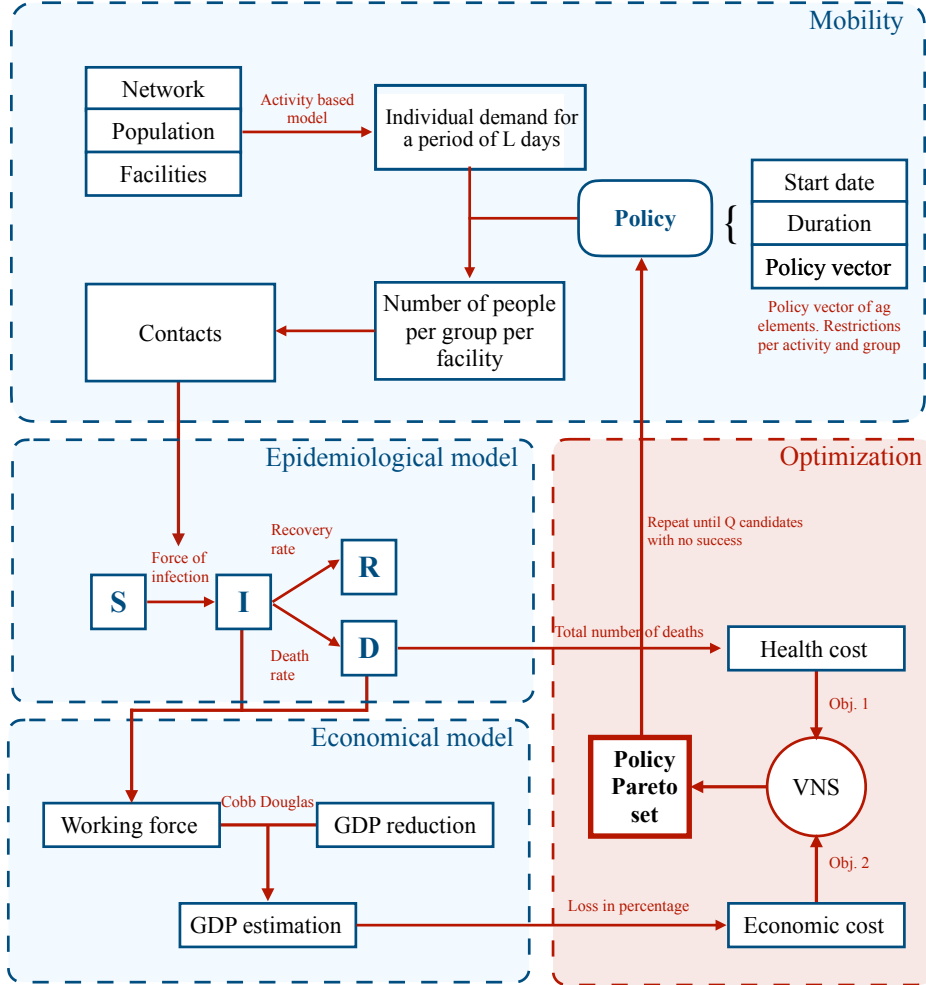


Figure 1: Dynamics of the framework

From this list, we derive the number of individuals for each facility  $f$  performing an activity  $a$ , each group  $g$  and each time interval  $t$  on day 0, the reference day:

$$N_{fagt}^0 = \sum_n \mathbb{1}[f_{nt} = f, g_n = g, a_{nt} = a], \quad (1)$$

where  $\mathbb{1}[\cdot]$  is one if all conditions are verified, and 0 otherwise. We derive the total number of people per facility by summing the number of individuals of each group  $g$  performing all the possible activities  $a$  in  $f$  at time  $t$  as:

$$N_{fgt}^0 = \sum_a N_{fagt}^0.$$

The number of individuals in a group  $g$  is therefore defined as

$$N_g = \frac{1}{T} \sum_t \sum_f N_{fgt}^0. \quad (2)$$

Note that we have dropped the index 0 representing the reference, as we assume that the global number of individuals in each group does not vary over time in the model.

In terms of infection information, we have at our disposal, for every day, the number  $\hat{y}_{gt}^i$  of infected individuals for each socio-economic group  $g$ . It is used to calibrate the parameters of the epidemiological model. Moreover, we need the initial values of the epidemiological situation: the number  $I_g^0$  of infected individuals per group  $g$  on day 0, the number  $R_g^0$  of recovered cases, and the number  $D_g^0$  of deceased individuals. The number  $S_g^0$  of susceptible cases is defined as everybody else:

$$S_g^0 = N_g - I_g^0 - R_g^0 - D_g^0.$$

In terms of economic situation, we need the GDP  $\hat{g}^0$  of the area under interest at day 0. We also need  $g_a^0$ , the contribution to the GDP of activity  $a$  on the reference day 0.

## 3.2 Modeling elements

The key elements of our modeling framework are: the number of contacts in the population organized into groups, the description of the epidemiological situation, the description of the restriction policies, and the force of infection, which serves as the link between the mobility of the individuals and the spread of the disease.

### 3.2.1 Number of contacts

The key indicator to model the spread of the disease on day 0 is the number of contacts generated by the activity schedules of the population. And in order to take into account the socio-economic characteristics of the individuals, we need such an indicator per group and per time interval. We define  $C_{fgjt}^0$  as the number of contacts between individuals from group  $g$  and group  $j$  in facility  $f$  at time  $t$ , which is, for each location, the number of individuals in one group multiplied by the number of individuals in the other group. If  $g$  and  $j$  happen to be the same group, we need to remove the contacts of an individual with herself, and divide by two to avoid double counting. Therefore,

$$C_{fgjt}^0 = \begin{cases} N_{fgt}^0(N_{fgt}^0 - 1)/2 & \text{if } g = j, \\ N_{fgt}^0 N_{fjt}^0 & \text{otherwise,} \end{cases} \quad (3)$$

where

$$N_{fgt}^0 = \sum_{\alpha} N_{f\alpha gt}^0.$$

The impact of the impact of  $C_{fgjt}^0$  on the spread of the infection is described in Subsection 3.2.4.

### 3.2.2 Epidemiological situation

The epidemiological situation of individual  $n$  on day  $\ell$  is characterized by a discrete variable  $H_{n\ell}$  which can take four values:

$$H_{n\ell} = \begin{cases} S & \text{if } n \text{ is susceptible on day } \ell, \\ I & \text{if } n \text{ is infected on day } \ell, \\ R & \text{if } n \text{ is recovered on day } \ell, \\ D & \text{if } n \text{ otherwise.} \end{cases} \quad (4)$$

The aggregate health state is captured by four continuous variables  $S_{g\ell}$ ,  $I_{g\ell}$ ,  $R_{g\ell}$ , and  $D_{g\ell}$  defining the total number of individuals in group  $g$  belonging to the corresponding compartment (Susceptible, Infected, Recovered, and Dead) on day  $\ell$ :

$$\begin{aligned} S_{g\ell} &= \sum_{n \in g} \mathbb{1} [H_{n\ell} = S], \\ I_{g\ell} &= \sum_{n \in g} \mathbb{1} [H_{n\ell} = I], \\ R_{g\ell} &= \sum_{n \in g} \mathbb{1} [H_{n\ell} = R], \\ D_{g\ell} &= \sum_{n \in g} \mathbb{1} [H_{n\ell} = D], \end{aligned}$$

such that  $S_{g\ell} + I_{g\ell} + R_{g\ell} + D_{g\ell} = N_g, \forall g, \ell$ .

### 3.2.3 Restriction policies

We are interested in analyzing the impact of lockdown policies that limit the number of individuals allowed in various categories of facilities. For instance, closing restaurants, or limiting the access to shops to a maximum number of individuals. A policy  $\Theta$  consists in applying a restriction factor to the different groups  $g$  and activities  $\alpha$ , between day  $\ell_u^p$  and day  $\ell_v^p$ , where

$$\ell_u^p \geq 0, \quad (5)$$

and

$$0 \leq \theta_{\alpha g \ell} \leq 1.$$

For instance, if the factor is set to zero, it means that the corresponding facilities  $\mathcal{F}_a$  are closed, and cannot be used by group  $g$  during that period, and 1 otherwise.

Therefore, the number of individuals of group  $g$  in facility  $f$  during each time intervals  $t$  of day  $\ell$  is imposed to be

$$N_{fgt}^\ell = \sum_a \theta_{ag\ell} N_{fagt}^0, \quad (6)$$

where  $N_{fagt}^0$  is defined by (1). This quantity represents the number of individuals of each group who used to travel and perform activities during the reference day, and are staying home on day  $\ell$  because of the restriction policies. There are two impacts of a policy. First, reducing the number of individuals reduces the number of contacts and, therefore, potential infections. In that case, the number of contacts between  $\ell_u^p$  and  $\ell_v^p$  is (3) where  $N_{fgt}^0$  is replaced by  $N_{fgt}^\ell$ , defined by (6):

$$C_{fgjt}^\ell = \begin{cases} N_{fgt}^\ell (N_{fgt}^\ell - 1)/2 & \text{if } g = j, \\ N_{fgt}^\ell N_{fjt}^\ell & \text{otherwise.} \end{cases} \quad (7)$$

The impact of that new contact matrix on the spread of the infection is described in Subsection 3.2.4. The second impact is economic. The working force is reduced by the policy, which has a direct impact on the GDP of the country. This reduction is due to mainly two factors: interruption of activities due to the government's decisions, and infected or deceased individuals who stop contributing to the work force. The modeling of this impact is described in Subsection 3.3.2.

### 3.2.4 Force of infection

The core of the model consists in predicting how contacts (characterized by the variable  $C_{fgjt}^\ell$ ) translate into infections. This is captured by a quantity called the ‘‘force of infection’’. For each day  $\ell$ , and each group  $g$ , we define  $\beta_{g\ell}$  as the ‘‘force of infection’’, that is the rate at which susceptible individuals of group  $g$  acquire an infectious disease, and can be represented by:

$$\beta_{g\ell} = \sum_f \sum_j \sum_t \rho_{gj} C_{fgjt}^0 \frac{I_{j(\ell^*-\nu)}}{N_j}, \quad (8)$$

where each term of the sum represents the infections caused by a different group  $j$ ,  $\rho_{gj}$  represents the proportion of contacts between  $g$  and  $j$  that translates into an actual infection, and  $I_{j(\ell^*-\nu)}$  is the number of infected individuals from group  $j$  at time  $\ell^* - \nu$ , where  $\nu$  is the incubation period. The parameters  $\rho_{gj}$  must be calibrated from data, as described in Appendix A.

### 3.3 Performance indicators

We are now interested in deriving global indicators corresponding a given scenario. In order to do this, we first capture the dynamics of the infection using an epidemiological model, described in Subsection 3.3.1. It allows to derive an indicator of the global sanitary situation. Then, we feed the outcome of this model into an economic model (described in Subsection 3.3.2) to derive a global economic indicator.

#### 3.3.1 Epidemiological model

The role of the epidemiological model is to capture the dynamics of the epidemic in the population. The reference state-of-art model for this phenomenon is called SIRD (Kermack et al., 1927). The SIRD model predicts the number of cases in the population using Ordinary Differential Equations (ODEs), with the implicit assumption that the underlying variables are continuous. Some versions of the model apply these equations on each group of the population (usually, segmented by age groups):

$$\begin{aligned}\frac{dS_{gl}}{dt} &= -\beta_{gl}S_{gl} \\ \frac{dI_{gl}}{ds} &= \beta_{gl}S_{gl} - \gamma_g I_{gl} - \mu_g I_{gl} \\ \frac{dR_{gl}}{ds} &= \gamma_g I_{gl} \\ \frac{dD_{gl}}{ds} &= \mu_g I_{gl},\end{aligned}$$

where  $\beta_{gl}$  is the force of infection defined by (8). In our context, with the variables capturing the epidemiological situation being discrete, we reformulate the ODEs as follows:

$$S_{g(\ell+1)} = S_{gl} - \beta_{gl}S_{gl} \quad \text{where } S_{gl} \geq 0, \quad (9)$$

$$I_{g(\ell+1)} = I_{gl} + \beta_{gl}S_{gl} - \gamma_g I_{gl} - \mu_g I_{gl} \quad \text{where } I_{gl} \geq 0, \quad (10)$$

$$R_{g(\ell+1)} = R_{gl} + \gamma_g I_{gl} \quad \text{where } R_{gl} \geq 0, \quad (11)$$

$$D_{g(\ell+1)} = D_{gl} + \mu_g I_{gl} \quad \text{where } D_{gl} \geq 0. \quad (12)$$

Note that the variables S, I, R and D stay non negative because the parameters  $\beta$ ,  $\gamma$  and  $\mu$  are between 0 and 1. This model can be used to derive an aggregate health cost  $\Upsilon$ , counting the death toll and the infected cases with severe symptoms during the period of interest:

$$\Upsilon = \sum_g \sum_{\ell} (D_{gl}). \quad (13)$$

### 3.3.2 Economic model

The economic situation on a given day  $\ell$  is captured by the Cobb-Douglas production function (Colas et al., 2021):

$$\Gamma_\ell = \zeta W_\ell^\lambda \quad (14)$$

where  $\zeta$  is a constant factor accounting, in particular, for the capital input,  $W_\ell$  is the working force at day  $\ell$ , and  $\lambda$  is the capital elasticity (Economy, 2020). At day 0,

$$W_0 = \alpha N, \quad (15)$$

where  $\alpha$  is the employment rate (Statista, 2020). Therefore, the value of  $\zeta$  can be derived from the observed GDP  $\widehat{g}^0$  using the following equation:

$$\ln \zeta = \ln \widehat{g}^0 - \lambda \ln(\alpha N). \quad (16)$$

We define  $\delta_\ell$  the reduction of the percentage of GDP due to the restrictions applied to the activities:

$$\delta_\ell = \sum_a \left[ \sum_g (1 - \theta_{ag\ell}) \frac{N_g}{N} \right] (\text{gdp})_a^0, \quad (17)$$

where  $(\text{gdp})_a^0$  is the contribution to the GDP of activity  $a$  on day 0. The working force on day  $\ell$  is defined as

$$W_\ell = \alpha(N^0 - M^\ell), \quad (18)$$

where

$$M^\ell = \sum_g I_{g\ell} + D_{g\ell}$$

is the number of individuals missing for the working force, because they are infected, and must stay home, or deceased, and  $\alpha$  is the employment rate. Therefore, the GDP on day  $\ell$  is defined as:

$$\Gamma_\ell = \zeta \delta_\ell W_\ell^\lambda, \quad (19)$$

where  $\zeta$  is defined by Equation (16). And the average GDP during the period of interest is

$$\Gamma = \frac{1}{L} \sum_\ell \Gamma_\ell. \quad (20)$$

To calculate the loss of GDP for every activity due to the unemployment given by the lockdown policies, the values of the vector of contribution to GDP  $(\text{gdp}_a^0)$

are taken from the literature (Janko et al., 2023). A significant challenge is the assumptions regarding the contribution of GDP for each group. Estimating the economic impact of various sectors or groups is not straightforward, especially in a dynamic global economy. Although we base our assumptions on the best available data and expert opinions, there is an inherent level of uncertainty. The potential discrepancies in these assumptions can lead to variations in the projected outcomes of our policies.

### 3.3.3 High-dimensional decision variable in policy formulation

The policy formulation within our multiobjective optimization framework is encapsulated by a high-dimensional decision variable, denoted as a tensor  $\Theta$ . This tensor  $\Theta$  includes elements  $\theta_{ag\ell}$  representing the level of restriction imposed for every activity  $\alpha$ , group  $g$ , and day  $\ell$  within the time interval from  $\ell_u^p$  to  $\ell_v^p$ . The tensor is structured such that:

$$\Theta = \{\ell_u^p, \ell_v^p, \theta_{ag\ell} \mid \forall g \in \mathcal{G}, \forall \alpha \in \mathcal{A}\}. \quad (21)$$

For days outside of the policy enforcement period, the restriction factors are set to 1, indicating no restrictions:

$$\theta_{ag\ell} = 1, \quad \forall g, \forall \alpha, \quad \text{for } \ell < \ell_u^p \text{ or } \ell > \ell_v^p. \quad (22)$$

This high-dimensional tensor allows for a tailored policy design, which is capable of capturing the relationship between different population segments, activities, and time intervals. The dimensionality of  $\Theta$  highlights the need for an algorithm that allows navigating through solutions and optimizing a wide policy space, thus facilitating the identification of targeted, effective, and potentially equitable interventions.

### 3.3.4 Summary

In summary, the models proceed as follows. From a given restriction policy  $p$ , we derive the number of individuals of group  $g$  in facility  $f$  during each time intervals  $t$  of day  $\ell$  using Equation (6). Then, we compute the contact matrix using Equation (7). The force of infection is derived from the contact matrix using Equation (8). The epidemiological model (9)–(12) is then applied to obtain the health situation during the period of interest. This is used to calculate two indicators:

- a health cost  $\Upsilon$ , defined by (13), and
- the average GDP  $\Gamma$ , defined by (20).

Finally, our multiobjective optimization problem can be written as:

$$\min [\Upsilon(\mathbf{p}), \Gamma(\mathbf{p})] \quad (23)$$

subject to:

$$(5), (6), (7), (8), (9)–(12).$$

In addition to the primary indicators of health and economic performance derived from our integrated epidemiological and activity-based models, it is possible to incorporate further indicators into our multi-objective optimization framework. For example, we can introduce a third objective focused on healthcare system capacity, with the aim of keeping hospitalizations within manageable limits to prevent healthcare system overload. This would involve adapting our epidemiological model to include a hospitalization compartment and stratifying the population by area. Subsequently, our optimization algorithm could identify local activity restriction policies that simultaneously minimize mortality, economic loss, and the number of hospital cases, ensuring that local healthcare systems remain within capacity. The adaptation of the compartmental model to include a hospitalization compartment and a segmentation based on the municipality of the individual allows for a local policy design that is responsive not only to global health and economic concerns, but also to the critical regional healthcare capacities.

### 3.4 Optimization

The above models allow for each restriction policy  $\mathbf{p}$  to derive two indicators: a health cost  $\Upsilon(\mathbf{p})$  and an economic indicator  $\Gamma(\mathbf{p})$ . These indicators play a significant role in optimizing policy decisions. However, the task of optimizing these parameters presents a significant challenge due to their conflicting nature and the high-dimensional complexity of the decision variable involved.

To address this complexity, the Variable Neighborhood Search (VNS) methodology and its various operators are introduced. VNS is a metaheuristic algorithm widely used to solve complex optimization problems. VNS (Mladenovic and Hansen, 1997; Ortelli et al., 2021) operates by exploring different neighborhoods around a current solution, adapting to the characteristics of the problem, and iteratively improving the solution. It is particularly effective for multi-objective optimization problems, such as the one at hand.

In the context of this multi-objective optimization problem involving health cost and GDP, VNS employs various operators to explore and refine policy solutions. The key operators used in VNS include move operators, which VNS uses to explore alternative policy solutions by modifying the restrictions in various ways to generate a set of diverse policies that need to be evaluated. Examples of these

operations include adding, removing, or adjusting specific restrictions in a policy. Additionally, VNS integrates local search operators that focus on refining a given policy within a specific neighborhood, aiming to improve it by making iterative, minor changes, and evaluating their effects on health costs and GDP. To avoid local optima, VNS uses perturbation strategies that inject a controlled amount of randomness into the search. This can involve altering the current policy or departing from a local minimum to inspect a different part of the solution space. An essential step in the process is the objective function evaluation, where VNS computes the health cost and GDP of each policy according to the set objectives, determining its quality and if it contributes to the Pareto optimal set.

The selection of VNS operators and their combination in the algorithm can substantially dictate its efficiency in discovering Pareto optimal policies. Since these two objectives are conflicting, we need to introduce the notion of dominance.

We say that policy  $p_1$  dominates policy  $p_2$ , if the corresponding health cost is lower and the GDP strictly greater

$$\Upsilon(p_1) \leq \Upsilon(p_2) \text{ and } \Gamma(p_1) > \Gamma(p_2),$$

or if the corresponding health cost is strictly greater and the GDP lower

$$\Upsilon(p_1) < \Upsilon(p_2) \text{ and } \Gamma(p_1) \geq \Gamma(p_2).$$

Note that the dominance relation is not complete. Indeed, if one policy is better for one criterion than another policy, but worse for the other criterion, none of the policies is dominating the other one.

Consider a set of policies  $\mathcal{P}$ , we say that policy  $p^*$  is Pareto optimal if it is not dominated by any policy in  $\mathcal{P}$ .

### 3.4.1 VNS input

The neighborhood structures  $\mathcal{H}_z(\Theta)$  in our VNS algorithm are defined on the basis of the size parameter  $z$ . Each structure represents a set of policy configurations accessible from the current solution  $\Theta$  using size operators  $z$ . We also define  $Q$  as the maximum number of unsuccessful candidates for each neighborhood structure.

$$\mathcal{H}_z(\Theta) = \{\Theta' \mid \Theta' \text{ is obtained from } \Theta \text{ using operators of size } z, \} \quad (24)$$

where  $z$  decides how much policies are modified, allowing varying levels of adjustment.

### 3.4.2 Customization of VNS operators

Our operators, designed to interact with  $\Theta$  and  $\mathcal{H}$ , include:

1. **Policy adjustment operators:** These operators modify the elements  $\theta_{agl}$  of  $\Theta$  to either increase or decrease the level of restriction for specific activities and groups. The operators adjust  $\theta_{agl}$  by a predefined step size  $z\delta$ . Where  $\delta$  is fixed to 10%. For instance, the increase policy operator modifies  $\theta_{agl}$  to  $\min(\theta_{agl} + z\delta, 1)$ , whereas the decrease policy operator updates it to  $\max(\theta_{agl} - z\delta, 0)$ . There are ag operators of this type for increasing the level of restriction and ag for decreasing them.
2. **Time adjustment operators:**
  - Increase/Decrease start time operator: These operators modify the policy's starting time  $\ell_u^p$ , either advancing or delaying the onset of policy enforcement. The increase start time operator modifies  $\ell_u^p$  to  $\max(1, \min(\ell_u^p + z, \ell_v^p))$ , whereas the decrease operator updates it to  $\max(1, \min(\ell_u^p - z, \ell_v^p))$ .
  - Increase/Decrease end time operator: Similarly, these operators adjust the policy's ending time  $\ell_v^p$ , extending or shortening the duration of policy application. The increase end time operator modifies  $\ell_v^p$  to  $\max(\ell_u^p, \min(\ell_v^p + z, L))$ , whereas the decrease operator updates it to  $\max(\ell_u^p, \min(\ell_v^p - z, L))$ .
  - Postpone policy operator: This operator advances both the starting and ending times of the policy enforcement period. The new starting time is calculated as  $\ell_u^{p'} = \max(1, \min(\ell_u^p + z, L))$ , and the new ending time is  $\ell_v^{p'} = \max(\ell_u^{p'}, \min(\ell_v^p + z, L))$ .
  - Anticipate policy operator: This operator moves the policy enforcement period earlier. It calculates the new starting time as  $\ell_u^{p'} = \max(1, \min(\ell_u^p - z, L))$ , and the new ending time as  $\ell_v^{p'} = \max(\ell_u^{p'}, \min(\ell_v^p - z, L))$ .
3. **Extreme policy operators:** These two operators set all  $\theta_{agl}$  values to the extremes, representing the broadest scope within  $\mathcal{H}$ . The first one sets all  $\theta_{agl}$  to 1, and the second sets all  $\theta_{agl}$  to 0.

### 3.4.3 Integration within the VNS framework

The VNS algorithm, through iterative navigation of  $\mathcal{H}$ , dynamically adjusts policy configurations:

- **Dynamic neighborhood search:** The algorithm picks and adapts randomly the neighborhood size  $z$  and applies it to the operators to refine  $\Theta$ .

- **Operator application:** Operators are applied to  $\Theta$ , according to the current neighborhood structure, creating new configurations  $\Theta'$ .
- **Evaluation and Update:** Configurations  $\Theta'$  are evaluated for their impact on health and economic outcomes, with the solution set updated to include only those enhancing the Pareto front.
- **Finalization:** When  $Q$  candidate solutions have been evaluated without success for a particular neighborhood structure  $z$ , the algorithm then shifts to the next structure,  $z + 1$ . This process continues until the final neighborhood structure,  $Z$ , is explored. The algorithm is designed to restart the entire process whenever it identifies an improved model.

## 4 Case study

In this section, we examine the outcomes of our study, focusing on the implications of various restrictions on both public health and economy. To conduct our analysis, we use a synthetic population that captures the activity-travel behavior within the canton of Vaud, Switzerland, sourced from a calibrated MATSim simulation output from ETH Zurich (Horl and Balac, 2021). These mobility data are complemented by aggregating open-source health data, categorized by age groups, including the positive, the negative, and the total tests performed by an age group  $g$  from mid-February 2020 to end-July 2020 (CloudPlatform, 2021). The calibration and validation of the model can be found in Appendix A of the paper.

Regarding parameter values, we choose  $\nu$  based on the "incubation period" (see Galmiche et al., 2023). The incubation period is known to be 5 days and is defined as the average number of days between an infection and a positive test. To calculate the loss of GDP for every activity due to the unemployment given by the lockdown policies, the values of the vector of contribution to GDP ( $\text{gdp}_a^0$ ) are taken from the literature (Janko et al., 2023). A significant challenge is the assumptions regarding the contribution of GDP for each group. Estimating the economic impact of various sectors or groups is not straightforward, especially in a dynamic global economy. Although we base our assumptions on the best available data and expert opinions, there is an inherent level of uncertainty. The potential discrepancies in these assumptions can lead to variations in the projected outcomes of our policies.

Our method takes into account the varied patterns of daily travel and activity among different population segments of the population, and it targets segment-specific actions that can benefit from that by limiting only when the restriction reduces mortality and/or economic loss. In our study, we examine the population in

four age groups: children (0-17 years), young adults (18-34 years), adults (35-64 years), and older adults (65 and older). This segmentation is chosen because age is the common attribute available in both health-related data and activity-travel behavior data sets. However, there are other segments that would be useful and interesting to analyze. For example, segment by the level of rurality of the area where people live, since this greatly affects how individuals travel, their daily routines, and most importantly, the amount of contacts per day. This type of segmentation would tailor local rules, allowing lighter restrictions with lower mortality and economic impact. Alternatively, we could group people by employment status, which could help decision-makers to organize better teleworking from home, and when people should go shopping, making sure the rules fit everyone’s situation, by keeping the mortality rate and economic loss low.

The findings presented in the following sections show the impact of various intervention strategies, underscoring the strengths of our targeted approach. Significantly, the outcomes of the Pareto front, which have been assessed using different initial values, consistently converge to the same solution. This convergence supports the stability of the Pareto front and its uniqueness, offering a reliable tool for decision-making. Furthermore, these outcomes can be effectively displayed on a dashboard, providing decision makers with a practical means to compare and contrast potential solutions.

## 4.1 Analysis on Reaction Times

This subsection illustrates the critical importance of reaction times in determining the range of Pareto optimal policy outcomes during a pandemic, in accordance with the results obtained by Aleta et al., 2020. Figure 2 presents the Pareto front of the optimization problem (23), where each dot corresponds to a Pareto optimal policy among all policies investigated by the algorithm. The Pareto front illustrates the trade-off between GDP loss and the number of deaths for various policy implementation scenarios. Each scenario considers a different starting time  $\ell_u^p$ , by modifying constraint (5). The plots capture the results of numerous simulations, with each point representing a specific combination of interventions and their corresponding impact on public health and the economy. Given the importance of starting time in the formulation of policies, it is observed that across various scenarios with predefined starting constraints, the Pareto optimal solutions consistently converge on the recommendation for immediate implementation.

In the 10-Day Scenario (red), policies begin after 10 days, representing an idealized quick response. The 20-Day Scenario (blue) has a 20-day delay, while the 30-Day Scenario (green) mirrors the response time seen in the pandemic’s initial wave. The 40-Day Scenario (yellow) denotes a 40-day delay, indicating a substantial delay in action. The Pareto front of each scenario is composed of

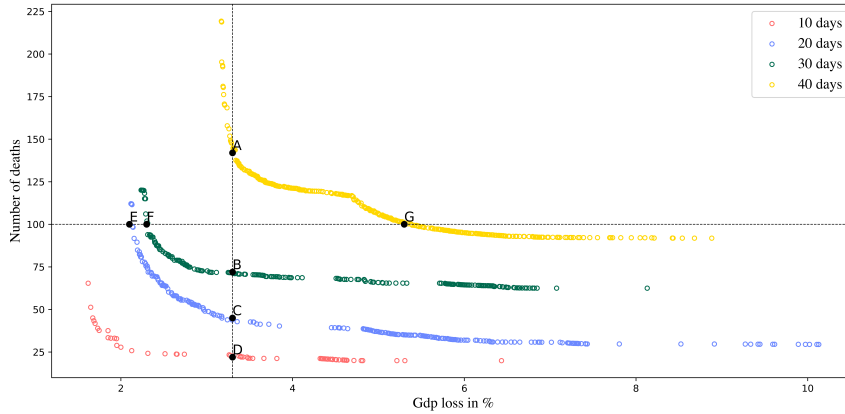


Figure 2: Reaction Time Impact on GDP Loss and Number of Deaths

different policy choices. A lower position on the y-axis indicates fewer deaths, whereas a position further to the right on the x-axis represents a higher GDP loss. A short reaction time, particularly within the initial 10 days, offers a variety of strategies that successfully minimize both the death toll and the economic loss. In this scenario, it is possible to achieve outcomes where GDP loss is restricted to approximately 1.5%, while the number of deaths remains below 40. On the other hand, as the reaction time increases to 40 days, the available policy options become severely limited, with no apparent solution capable of limiting the number of deaths to less than 100 or a GDP or a GDP loss greater than 3%. With this information, we can generate a dashboard similar to Table 2 that policy makers could use.

Table 2 clearly shows the delicate balance that policy makers must achieve in the timing of their responses to a health crisis. In Policy A we observe that while the GDP loss remains constant, the human cost in terms of deaths can vary dramatically, underscoring that economic measures are intrinsically linked to health outcomes. The stability of GDP loss across varying policy reaction times is particularly sensitive, as the productivity and contributions of individuals who are infected or have unfortunately died are directly factored into the economic performance indicator. This is because the loss of workforce due to illness or death can have a great effect on GDP, beyond the immediate impact of restrictions on economic activities. Each policy adjustment, such as opening or closing sectors like education or shopping, is a strategic move to minimize this dual impact. For example, in Policy B, for Group 2, leisure remains closed and education is partially open compared to Policy C, indicating a possible hybrid model of online and in-person activities. On the other hand, group 3 has leisure activities open to

Policies	Duration	Groups	Activities					GDP Loss	Deaths
			Home	Leisure	Work	Shop	Education		
Policy D	116	Group 1	1.0	1.0	1.0	1.0	0.4	3.3	21.27
		Group 2	1.0	0	0.0	0.45	0		
		Group 3	1.0	0.0	0	0.0	1.0		
		Group 4	1.0	1.0	1.0	1.0	1.0		
Policy C	86	Group 1	1.0	1.0	1.0	1.0	0.0	3.3	43.84
		Group 2	1.0	0.0	0.0	1.0	0.0		
		Group 3	1.0	0.0	0.0	0.15	0.0		
		Group 4	1.0	0.1	1.0	1.0	1.0		
Policy B	77	Group 1	1.0	1.0	1.0	1.0	0.0	3.3	71.01
		Group 2	1.0	0.0	0.0	0.5	0.0		
		Group 3	1.0	0.0	0.0	0.25	0.15		
		Group 4	1.0	0.7	1.0	1.0	1.0		
Policy A	50	Group 1	1.0	1.0	1.0	1.0	0.1	3.3	128.25
		Group 2	1.0	0.0	0.0	1.0	0.0		
		Group 3	1.0	0.0	0.0	0.3	0.6		
		Group 4	1.0	0.0	1.0	1.0	1.0		

Table 2: Summary of policy configurations and their impacts over different reaction times - constant GDP loss

children and the elderly but closed to all adults, compared to Policy C, suggesting relaxation in certain areas to maintain economic stability. Continuing the narrative established in the previous table, where we examined the impact of different policy reaction times on GDP loss, Table 3 presents a complementary perspective. Here, we consider a limit of a maximum of 100 casualties acceptable, analyze how our tool proposes policy adjustments, and see the influence of economic activities on constant health outcomes. Similarly to earlier findings, where consistent GDP loss across various durations highlighted the intertwining of economic and health consequences. This table underscores the policy changes required to maintain a fixed number of casualties. For example, in Policy E, we observe that group 1 faces a 50% restriction in education, while group 4 is subject to a 70% reduction in shopping, delineating a strategic calibration of restrictions across different sectors. This reflects the observation of the previous table, such as the reopening of 15% of the education facilities in Policy F for group 2, showing an adaptive mix of online and offline modes. Relaxation of work and leisure activities for group 3 in the same reaction time scenario also mirrors this approach, a strategic shift in policy to preserve economic equilibrium while keeping health impacts constant. These correlations between the two tables enrich our understanding of the complex and dynamic nature of policy making in crisis situations, where the goal transcends mere balancing and ventures into optimizing the delicate interplay between public health and economic health. This comparison shows how important it is to act quickly and make guided decisions during a pandemic. It

Policies	Duration	Groups	Activities					GDP Loss	Deaths
			Home	Leisure	Work	Shop	Education		
Policy E	60	Group 1	1.0	1.0	1.0	1.0	0.5	3.94	98.57
		Group 2	1.0	0.0	0.0	1.0	0.0		
		Group 3	1.0	0.0	0.0	1.0	1.0		
		Group 4	1.0	1.0	1.0	0.7	1.0		
Policy F	57	Group 1	1.0	1.0	1.0	1.0	0.45	4.11	100.67
		Group 2	1.0	0.15	0.0	1.0	0.0		
		Group 3	1.0	0.0	0.0	1.0	1.0		
		Group 4	1.0	1.0	1.0	0.45	1.0		
Policy G	52	Group 1	1.0	0.7	1.0	1.0	0.0	6.94	99.34
		Group 2	1.0	0.0	0.0	0.9	0.0		
		Group 3	1.0	0.0	0.0	0.0	0.0		
		Group 4	1.0	0.0	1.0	0.25	0.45		

Table 3: Summary of policy configurations and their impacts over different reaction times - constant deaths

also highlights how being prepared and able to adapt quickly in how we respond can help to lessen the effects on both people’s health and the economy.

## 4.2 Analysis of Policy Scenarios and Their Impacts

In this subsection, we analyze various policies and their impacts. We explore the contrast between the real policy implemented and three Pareto optimal policies proposed by our model, highlighting the implications for public health and the economy.

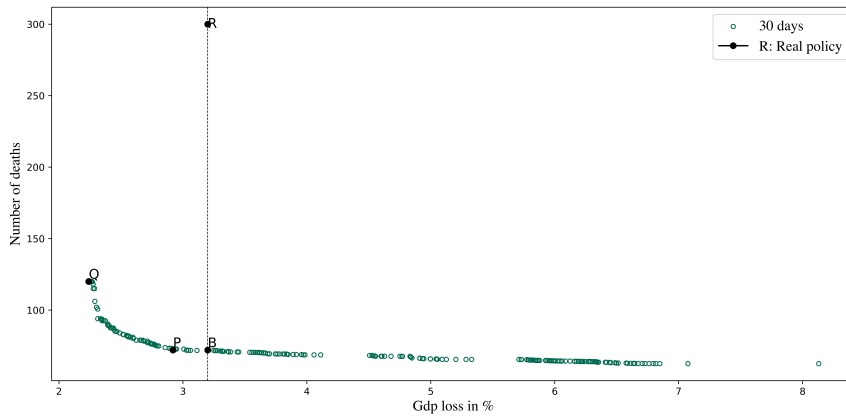


Figure 3: Analysis of Policy Scenarios and Their Impacts

Figure 3 provides a visual representation of the real policy, marked by an or-

ange point, and serves as a reference point, reflecting a baseline scenario with significant economic and health consequences (Office, 2022). Figure 4 represents a series of spider charts that illustrate multiple policies with respect to five different activities: home, recreation, work, shop, and education. The spider chart is designed in a polygon frame, where each axis of the chart corresponds to one of these categories. The data for each policy are represented as a filled area plot in the spider chart, where the magnitude along each axis denotes the restriction of the policy for that activity. Combining the information from Figure 3 and Figure 4 we observe how Policy S, emphasizing health, applies varying restrictions for different groups: The first group experiences full opening for work and shopping, but fully closing for leisure and education, reflecting a focus on maintaining essential economic activities while limiting social interactions. The second group faces total closure in leisure and work and reduces shopping activities to 40%, indicating a more stringent approach, while the third group faces total closure in education. In contrast, Policy P, with an economic focus, shows a more balanced approach, allowing more activities such as full opening for work and shopping for the first group, but with moderate leisure in 15% and education at 45% for the second group. This suggests an attempt to sustain economic functions while controlling high-risk activities. Policy Q, which aims for a balance, allows increased activity in education 60% for the first group, indicating recognition of the long-term importance of education in conjunction with immediate health concerns.

In all, these policies underline the delicate trade-off between GDP and economic and health considerations, and each group faces various restrictions based on its profile and the broader strategy of each policy.

### **4.3 Comparison of Aggregated vs. Disaggregated Policies**

Modern policymaking, especially in response to global challenges, requires a nuanced approach due to the difficulty in creating strategies that effectively serve diverse populations and sectors. The debate between aggregated and disaggregated policies brings to light the complexities involved in finding strategies that target different populations and sectors.

Aggregated policies, often referred to as "one-size-fits-all" approaches, offer a uniform solution. They are generally easier to implement and monitor, given their broad application. However, they may not always meet the specific needs of individual sectors or groups, which can lead to inefficiencies or unintended consequences.

Disaggregated policies allow for tailored strategies. They take into account the unique characteristics and needs of different sectors or groups. By being more targeted, they can potentially offer more effective solutions, especially in situations where blanket policies might be counterproductive. Figure 5 shows the Pareto

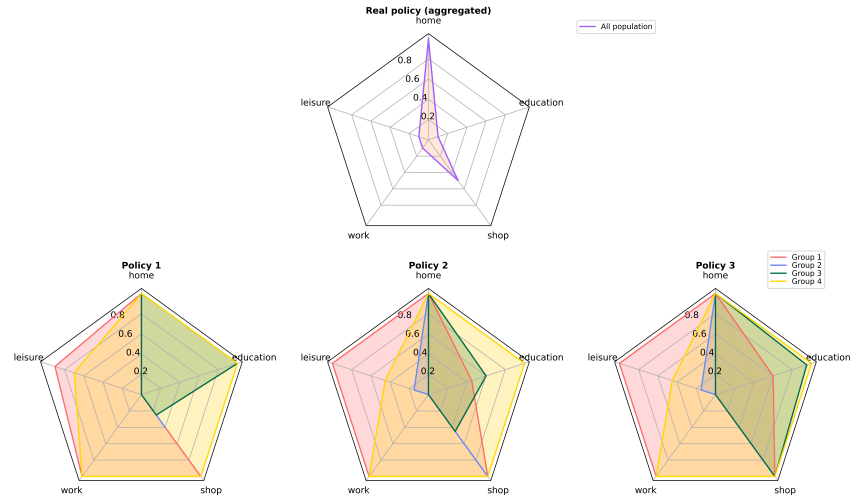


Figure 4: Comparison of Policy Restrictions Using Spider Plots

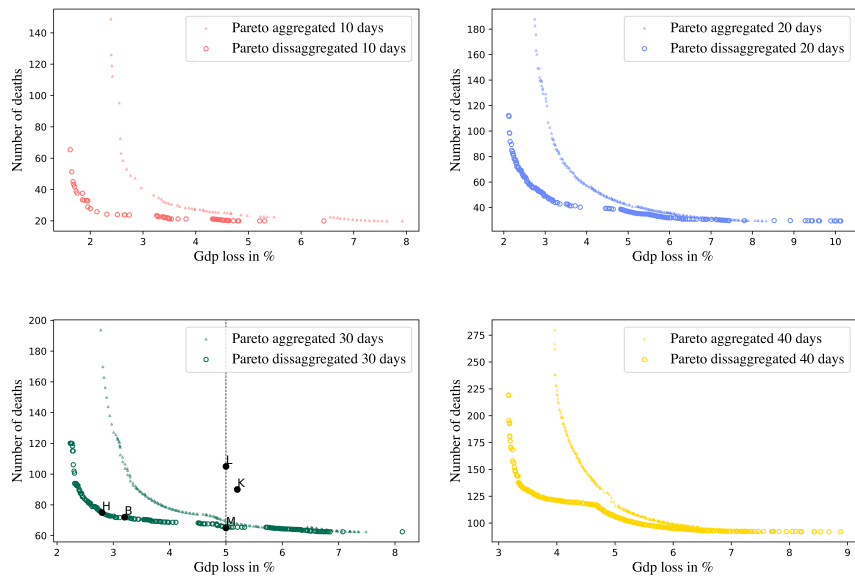


Figure 5: Pareto Fronts for Aggregated and Disaggregated Policies

fronts for aggregated and disaggregated policies over a specific reaction time. The figure underscores the potential gains from customized policies. We observe that,

while aggregated policies might offer certain benefits in terms of simplicity and broad applicability, disaggregated policies can provide more optimized outcomes for specific scenarios, for example when we deal with a high reaction time. If we observe the 30-day scenario, we draw a vertical line at GDP loss 5% to compare the disaggregated and aggregated approach to implement policies. When we look at it, we observe that Policy M leads to far fewer deaths when compared to Policy L, from 105 to 65. This means 5 more lives for every 100,000 people while assuming the same GDP loss. The decrease in human loss is achieved by applying stricter measures to young adults and adults, and allowing children and the elderly to do most of the activities. Moreover, Policy H proposes optimal trade-off policies that only cause a 2.8% loss to the economy, but still keep deaths at 75 for the disaggregated case. For the aggregated approach, the best trade-off that can be achieved is 90 deaths with a 5.2% loss to the economy (Policy K).

In conclusion, our results suggest that having a more focused policy can save more lives and also be better for the economy. Although both aggregated and disaggregated policies have their benefits, the choice between them should be informed by the specific challenges at hand, the desired outcomes, and the nuances of the sectors or groups in question. Furthermore, our data set for epidemiological analysis was exclusively classified by age groups, which limited our policy formulation strictly to age-related considerations. For example, by incorporating nonsensitive attributes such as employment status, we would be able to more accurately calibrate the impact on GDP from various activities, since the amount of money spent by the different groups on the different activities is different. By having this information, we could better tailor the policies.

## 5 Conclusions

In conclusion, Our study provides a tool for designing policies in such situations, emphasizing the value of segmentation in formulating targeted measures. Our research in the canton of Vaud, Switzerland, accentuates the importance of quick and precise policy responses during health crises. These strategies not only fortify public health, but also attenuate economic repercussions, ensuring a balanced allocation of impact in times of crisis. The rapidity of policy decisions, particularly at the outset of an outbreak, offers a broad spectrum of options for balancing health risks and economic stability. However, delayed responses can critically constrain these choices, underscoring the need for targeted policy approaches.

Future research could involve deepening demographics, such as employment status, to reveal a wider range of policy options. For instance, introducing time-specific policies tailored to different population segments, like allocating distinct shopping hours for employed and unemployed individuals, could elevate the pre-

cision and impact of these policies. This approach would retain the original model's optimization flexibility while ensuring equitable protection for all societal segments. Additionally, while our focus was primarily on policy effectiveness, the aspects of fairness, equity, and the potential resistance of the population to certain policies, although outside the scope of this paper, would be undoubtedly crucial for future investigations. These elements are essential to ensure not just the efficacy but also the societal acceptability and ethical soundness of policy measures. Unfortunately, our study dealt with constraints such as data accessibility and the inevitable assumptions we had to incorporate. This underlies the ongoing need to validate, reassess, and update our findings with evolving data.

Implementing these sophisticated policies in real-world scenarios calls for robust data infrastructure and collaborative synergy between researchers, health officials, and policymakers. The integration of advanced predictive tools, like machine learning algorithms, could further enhance our policy formulation tool, enabling more adaptive and responsive strategies. Additionally, considering the behavioral and psychological impacts of policy changes on the population could yield more holistic and effective interventions.

As we deal with the multifaceted impacts of the COVID-19 pandemic and prepare for future challenges, our work stands as a guiding principle, emphasizing the importance of flexible policy making.

## **Declaration of generative AI and AI-assisted technologies in the writing process**

During the preparation of this work the authors used OpenAI in order to paraphrase and check grammar and spelling. After using this tool/service, the authors reviewed and edited the content as needed and take full responsibility for the content of the publication.

## **References**

- Acemoglu, D., Chernozhukov, V., Werning, I. and Whinston, M. D. (2020). Optimal Targeted Lockdowns in a Multi-Group SIR Model.  
**URL:** <https://www.nber.org/papers/w27102>
- Aleta, A., Martin-Corral, D., Bakker, M. A., y Piontti, A. P., Ajelli, M., Litvinova, M., Chinazzi, M., Dean, N. E., Halloran, M. E., Longini, I. M., Pentland, A., Vespignani, A., Moreno, Y. and Moro, E. (2020). Quantifying the importance and location of SARS-CoV-2 transmission events in large metropoli-

- tan areas, preprint, *Epidemiology*.  
**URL:** <http://medrxiv.org/lookup/doi/10.1101/2020.12.15.20248273>
- Brotherhood, L., Kircher, P., Santos, C. and Tertilt, M. (2020). An Economic Model of the COVID-19 Epidemic: The Importance of Testing and Age-Specific Policies.
- Calderon Peralvo, F., Cazorla Vanegas, P. and Avila-Ordóñez, E. (2022). A systematic review of COVID-19 transport policies and mitigation strategies around the globe, *Transportation Research Interdisciplinary Perspectives* **15**: 100653.  
**URL:** <https://www.sciencedirect.com/science/article/pii/S2590198222001142>
- Chang, S., Pierson, E., Koh, P. W., Gerardin, J., Redbird, B., Grusky, D. and Leskovec, J. (2021). Mobility network models of COVID-19 explain inequities and inform reopening, *Nature* **589**(7840): 82–87.  
**URL:** <http://www.nature.com/articles/s41586-020-2923-3>
- Chari, V. V., Kirpalani, R. and Phelan, C. (2020). The Hammer and the Scalpel: On the Economics of Indiscriminate versus Targeted Isolation Policies during Pandemics. Institution: Staff Report Type: preprint.  
**URL:** <https://researchdatabase.minneapolisfed.org/concern/publications/n870zr009>
- Chen, V. C. P., Zhou, Y., Ghasemi, Y. and Guild, J. B. (2022). An Optimization Framework to Study the Balance Between Expected Fatalities Due to COVID-19 and the Reopening of U.S. Communities, *IEEE Transactions on Automation Science & Engineering* pp. 586–602.  
**URL:** <https://doi.org/10.1109/TASE.2021.3119930>
- CloudPlatform, G. (2021). Google Covid data.  
**URL:** <https://github.com/GoogleCloudPlatform/covid-19-open-data/blob/main/docs/table-epidemiology.md>
- Colas, C., Hejblum, B., Rouillon, S., Thiebaut, R., Oudeyer, P.-Y., Moulin-Frier, C. and Prague, M. (2021). EpidemiOptim: A Toolbox for the Optimization of Control Policies in Epidemiological Models, *Journal of Artificial Intelligence Research* **71**: 479–519.  
**URL:** <https://jair.org/index.php/jair/article/view/12588>
- Economy, G. (2020). Switzerland Trade openness. data, chart.  
**URL:** [https://www.theglobaleconomy.com/switzerland/trade\\_openness/](https://www.theglobaleconomy.com/switzerland/trade_openness/)

- Eubank, S., Guclu, H., Anil Kumar, V. S., Marathe, M. V., Srinivasan, A., Toroczkai, Z. and Wang, N. (2004). Modelling disease outbreaks in realistic urban social networks, Nature **429**(6988): 180–184. Number: 6988  
 Publisher: Nature Publishing Group.  
**URL:** <https://www.nature.com/articles/nature02541>
- Filho, T. M. R., Mendes, J. F. F., Murari, T. B., Filho, A. S. N., Cordeiro, A. J. A., Ramalho, W. M., Scorza, F. A., Almeida, A.-C. G. and Moret, M. A. (2022). Optimization of COVID-19 vaccination and the role of individuals with a high number of contacts: A model based approach, PLOS ONE **17**(3): e0262433. Publisher: Public Library of Science.  
**URL:** <https://journals.plos.org/plosone/article?id=10.1371/journal.pone.0262433>
- Galmiche, S., Cortier, T., Charmet, T., Schaeffer, L., Cheny, O., Platen, C. v., Levy, A., Martin, S., Omar, F., David, C., Mailles, A., Carrat, F., Cauchemez, S. and Fontanet, A. (2023). SARS-CoV-2 incubation period across variants of concern, individual factors, and circumstances of infection in France: a case series analysis from the ComCor study, The Lancet Microbe **4**(6): e409–e417. Publisher: Elsevier.  
**URL:** [https://www.thelancet.com/journals/lanmic/article/PIIS2666-5247\(23\)00005-8/fulltext](https://www.thelancet.com/journals/lanmic/article/PIIS2666-5247(23)00005-8/fulltext)
- Ghamizi, S., Rwemalika, R., Veiber, L., Cordy, M., Bissyande, T. F., Papadakis, M., Klein, J. and Traon, Y. L. (2020). Data-driven Simulation and Optimization for Covid-19 Exit Strategies. arXiv:2006.07087 [physics, q-bio].  
**URL:** <http://arxiv.org/abs/2006.07087>
- Horl, S. and Balac, M. (2021). Synthetic population and travel demand for Paris and Ile-de-France based on open and publicly available data, Transportation Research Part C: Emerging Technologies **130**: 103291.  
**URL:** <https://linkinghub.elsevier.com/retrieve/pii/S0968090X21003016>
- Janko, V., Rescic, N., Vodopija, A., Susic, D., De Masi, C., Tusar, T., Gradisek, A., Vandepitte, S., De Smedt, D., Javornik, J., Gams, M. and Lustrek, M. (2023). Optimizing non-pharmaceutical intervention strategies against COVID-19 using artificial intelligence, Frontiers in Public Health **11**.  
**URL:** <https://www.frontiersin.org/articles/10.3389/fpubh.2023.1073581>
- Kermack, W. O., McKendrick, A. G. and Walker, G. T. (1927). A contribution to the mathematical theory of epidemics, Proceedings of the Royal Society of London. Series A, Containing Papers of a Mathematical and Physical Character **115**(772): 700–721. Publisher: Royal Society.  
**URL:** <https://royalsocietypublishing.org/doi/10.1098/rspa.1927.0118>

- Kerr, C. C., Stuart, R. M., Mistry, D., Abeysuriya, R. G., Hart, G., Rosenfeld, K., Selvaraj, P., Nunez, R. C., Hagedorn, B., George, L., Izzo, A., Palmer, A., Delport, D., Bennette, C., Wagner, B., Chang, S., Cohen, J. A., Panovska Griffiths, J., Jastrzebski, M., Oron, A. P., Wenger, E., Famulare, M. and Klein, D. J. (2020). Covasim: an agent-based model of COVID-19 dynamics and interventions. Pages: 2020.05.10.20097469.  
**URL:** <https://www.medrxiv.org/content/10.1101/2020.05.10.20097469v1>
- Mladenovic, N. and Hansen, P. (1997). Variable neighborhood search, Computers & Operations Research **24**(11): 1097–1100.  
**URL:** <https://www.sciencedirect.com/science/article/pii/S0305054897000312>
- Molloy, J., Schatzmann, T., Schoeman, B., Tchervenkov, C., Hintermann, B. and Axhausen, K. W. (2021). Observed impacts of the Covid-19 first wave on travel behaviour in Switzerland based on a large GPS panel, Transport Policy **104**: 43–51.  
**URL:** <https://www.sciencedirect.com/science/article/pii/S0967070X21000159>
- Muller, S. A., Balmer, M., Charlton, B., Ewert, R., Neumann, A., Rakow, C., Schlenther, T. and Nagel, K. (2020). Using mobile phone data for epidemiological simulations of lockdowns: government interventions, behavioral changes, and resulting changes of reinfections, preprint, Epidemiology.  
**URL:** <http://medrxiv.org/lookup/doi/10.1101/2020.07.22.20160093>
- Nguyen, T. K., Hoang, N. H., Currie, G. and Vu, H. L. (2022). Enhancing Covid-19 virus spread modeling using an activity travel model, Transportation Research Part A: Policy and Practice **161**: 186–199.  
**URL:** <https://linkinghub.elsevier.com/retrieve/pii/S0965856422001173>
- Office, F. S. (2022). Gross domestic product per canton and region.  
**URL:** <https://www.bfs.admin.ch/bfs/en/home/statistiken/volkswirtschaft/volkswirtschaftliche-gesamtrechnung/bruttoinlandprodukt-kanton.html>
- Ortelli, N., Hillel, T., Pereira, F. C., de Lapparent, M. and Bierlaire, M. (2021). Assisted specification of discrete choice models, Journal of Choice Modelling **39**: 100285.  
**URL:** <https://linkinghub.elsevier.com/retrieve/pii/S175553452100018X>
- Qian, X. and Ukkusuri, S. V. (2021). Connecting urban transportation systems with the spread of infectious diseases: A Trans-SEIR modeling approach, Transportation Research Part B: Methodological **145**: 185–211.  
**URL:** <https://linkinghub.elsevier.com/retrieve/pii/S0191261521000175>

- Queiroz, M. M., Ivanov, D., Dolgui, A. and Fosso Wamba, S. (2022). Impacts of epidemic outbreaks on supply chains: mapping a research agenda amid the COVID-19 pandemic through a structured literature review, Annals of Operations Research **319**(1): 1159–1196.
- Statista (2020). Switzerland - Unemployment rate 2021.  
**URL:** <https://www.statista.com/statistics/263707/unemployment-rate-in-switzerland/>
- Tirachini, A. and Cats, O. (2020). COVID-19 and Public Transportation: Current Assessment, Prospects, and Research Needs, Journal of Public Transportation **22**(1).  
**URL:** <https://scholarcommons.usf.edu/jpt/vol22/iss1/1>
- Xi, H., Li, Q., Hensher, D. A., Nelson, J. D. and Ho, C. (2023). Quantifying the impact of COVID-19 on travel behavior in different socio-economic segments, Transport Policy **136**: 98–112.  
**URL:** <https://linkinghub.elsevier.com/retrieve/pii/S0967070X23000732>
- Yaesoubi, R., Havumaki, J., Chitwood, M., Menzies, N., Gonsalves, G., Salomon, J., Paltiel, A. and Cohen, T. (2021). Adaptive Policies to Balance Health Benefits and Economic Costs of Physical Distancing Interventions during the COVID-19 Pandemic, Medical Decision Making **41**: 0272989X2199037.
- Yasmin, F., Morency, C. and Roorda, M. (2015). Assessment of spatial transferability of an activity-based model, TASHA, Transportation Research Part A Policy and Practice **78**: 200–213.

## A Calibration of the epidemiological model

In order to calibrate the parameters  $\rho_{gj}$  of model (8), we need:

- $N_g$  the number of individuals in each group (2),
- $C_{fgjt}^0$  the number of contacts for the reference day (3),
- $S_g^0, I_g^0, R_g^0$  and  $D_g^0$ , the initial values of the epidemiological model, as discussed in subsection 3.1,
- $\hat{y}_{g\ell}^i$  the observed number of daily infections per group.

The parameters  $\rho_{gj}$  are obtained by solving the following least-squares problem:

$$\min_{\rho, S, I, R, D} \sum_{g=1}^G \sum_{\ell=6}^{L-1} \left( \hat{y}_{g\ell}^i - S_{g\ell} \frac{1}{T} \sum_f \sum_h \sum_t \rho_{gj} C_{fgjt}^0 \frac{I_j^{(\ell-5)}}{N_j} \right)^2 \quad (25)$$

subject to:

$$1 \geq \rho_{gj} \geq 0, \quad g, h = 1, \dots, G, \quad (26)$$

$$S_{g\ell} + I_{g\ell} + R_{g\ell} + D_{g\ell} = N_g, \quad g = 1, \dots, G, \ell = 1, \dots, L, \quad (27)$$

$$S_{g(\ell+1)} = S_{g\ell} - \beta_{g\ell} S_{g\ell}, \quad g = 1, \dots, G, \ell = 0, \dots, L-1, \quad (28)$$

$$I_{g(\ell+1)} = I_{g\ell} + \beta_{g\ell} S_{g\ell} - \gamma_g I_{g\ell} - \mu_g I_{g\ell}, \quad g = 1, \dots, G, \ell = 0, \dots, L-1, \quad (29)$$

$$R_{g(\ell+1)} = R_{g\ell} + \gamma_g I_{g\ell}, \quad g = 1, \dots, G, \ell = 0, \dots, L-1, \quad (30)$$

$$D_{g(\ell+1)} = D_{g\ell} + \mu_g I_{g\ell}, \quad g = 1, \dots, G, \ell = 0, \dots, L-1, \quad (31)$$

where the vectors  $S, I, R,$  and  $D$  contain the variables of the epidemiological model for each group and each day  $\ell = 1, \dots, L$ .

An important simplification in our model is the assumption that the parameter  $\rho_{gj}$  is independent of  $j$  and only a function of  $g$ . This means that we consider the contact rate to be dependent only on the characteristics of the group in question. This assumption is justified by the observation that social behaviors and interactions, which largely influence the contact rates, are more strongly dictated by group characteristics (such as age, occupation, social habits) rather than by the characteristics of the individual you are encountering.

To enhance the robustness of our model, we extend the calibration of the parameters  $\rho_{gj}$  beyond a single region. Specifically, we solve the aforementioned least-squares problem for multiple cantons. This approach allows us to test the generalizability of our model in different demographic and geographic contexts. The primary assumption here is that the contact rate parameters  $\rho_{gj}$ , although dependent on the group  $g$ , remain consistent in different cantons. This assumption

is based on the premise that the probability of contracting a disease given contact depends mainly on the health characteristics of the individual and, therefore, does not significantly vary across regions, especially within the same cultural and socioeconomic context.

## A.1 Calibration Results

After fitting the epidemiological model using the available data from the cantons with a higher population number, the parameters  $\rho_{gj}$  are derived.

### A.1.1 Optimized Parameters

Table 4 provides an overview of the calibrated parameters for each group.

Index	Canton	$\rho_{1j} \times 10^{-6}$	$\rho_{2j} \times 10^{-6}$	$\rho_{3j} \times 10^{-6}$	$\rho_{4j} \times 10^{-6}$
0	BE	86.506	15.314	37.327	65.708
1	NE	15.080	38.194	98.968	17.323
2	TI	94.906	32.254	6.794	80.611
4	VS	45.063	16.365	21.907	54.818
5	ZH	24.909	49.873	72.837	51.205

Table 4: Calibrated values of  $\rho_{gj}$  for each group  $g$ .

### A.1.2 Goodness-of-Fit

A comparison between the observed data and the model output, using the optimized parameters, is shown in Figure 6. The model matches closely to the distribution followed by the observed epidemic curves across different cantons. Note that the discrepancy observed in the image of the distributions can be attributed to insufficient testing of the population during the initial wave of COVID-19. As a result, the recorded data is approximately between 10% and 30% less than the actual figures. This implies that for every 100 people who were infected, only 90 to 70 were actually tested.

## A.2 Validation of the Epidemiological Model

Upon simulating the epidemic curve using our model, we observe a reasonable approximation between the predicted counts and the observed data in Vaud. This outcome not only validates the effectiveness of our model but also reinforces the

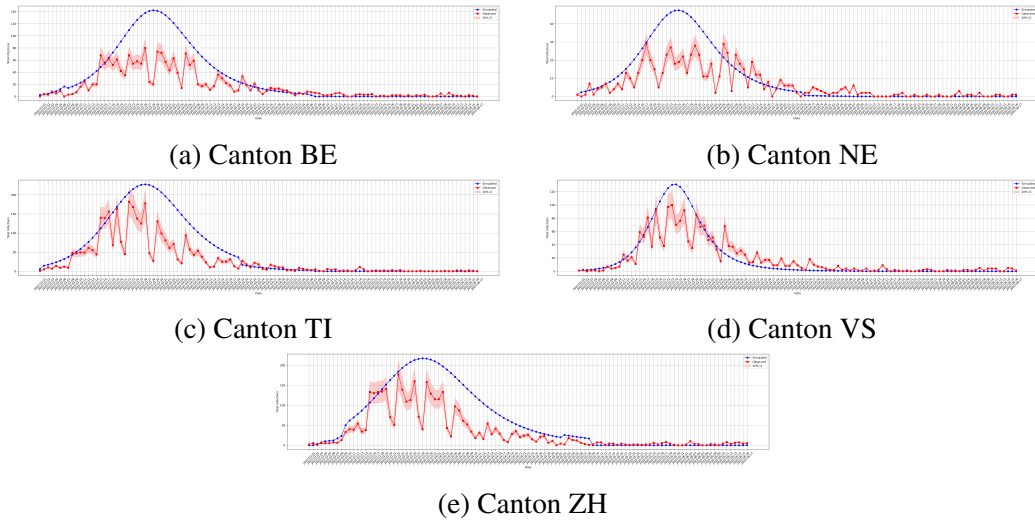


Figure 6: Comparison of observed and modeled epidemic curves using calibrated parameters for various cantons.

soundness of the underlying assumptions. The assumptions made about the contact rate parameter  $\rho$ , recovery time, mortality rate, and other epidemiological factors appear to hold true in the context of Vaud.

### A.2.1 Validation Approach

The model is trained using the averaged data from all cantons excluding Vaud. It is then used to simulate the epidemic curve in Vaud, and the resulting simulated curve is compared to the real observed data from Vaud.

### A.2.2 Validation Outcome

Upon simulating the epidemic curve using our model, we observe a reasonable approximation between the predicted counts and the observed data in Vaud. The successful alignment of the model's predictions with actual data suggests that the simplifications and generalizations inherent in our model do not significantly detract from its accuracy and applicability. In particular, the assumption that  $\rho$  is consistent across different cantons and independent of  $j$  is supported by the model's performance. Similarly, the estimations of recovery and mortality rates, integral to the epidemiological model, are substantiated through this validation process.

This concordance indicates that our model, despite its abstractions, captures the essential dynamics of the epidemic effectively. It provides a reliable tool for

understanding and predicting the spread of the disease, thereby aiding in informed decision-making for public health interventions.

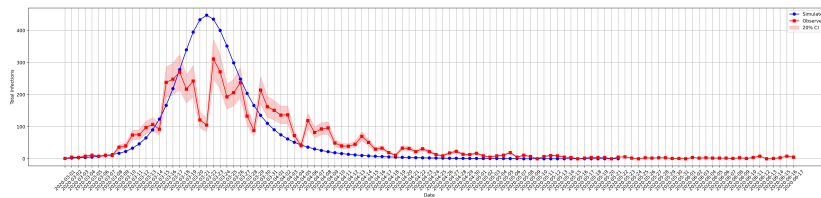


Figure 7: Comparison of simulated and actual epidemic curves for Vaud.

## Notation

Variable	Concept	Type
$T$	numbers of time intervals within a day	discrete
$L$	number of days	discrete
$G$	number of groups	discrete
$N$	number of individuals	discrete
$A$	number of activities	discrete
$C$	number of contacts	discrete
$I$	number of infected individuals	discrete
$S$	number of susceptible individuals	discrete
$R$	number of recovered individuals	discrete
$D$	number of deceased individuals	discrete
$M^\ell$	number of individuals missing for the working force at day $\ell$	discrete
$t$	time interval	index
$g, j$	group	index
$n$	individual	index
$a$	activity	index
$\ell$	day	index
$f$	facility	index
$\mathcal{F}$	set of locations	set
$\mathcal{F}_a$	set of locations	set
$\hat{y}_{g\ell}^i$	observed number of daily infections	data discrete
$\hat{y}^g$	GDP before the pandemic	CHF
$\ell_u^p$	beginning of policy p	index
$\ell_v^p$	end of policy p	index
$W_\ell$	number of individuals contributing to the working force on day $\ell$	integer
$\Gamma_\ell$	GDP on day $\ell$	CHF
$\text{gdp}_a^0$	contribution of the GDP of activity $a$ on day 0	CHF
$\theta_p$	restriction factor for policy p	continuous decision variable
$\alpha$	employment rate	
$\zeta$	Cobb-Douglas constant	
$\lambda$	Cobb-Douglas exponent	
$\beta_{g\ell}$	Force of infection	
$\rho_{gj}$	Infection from contact between $g$ and $j$	
$\delta_g$	recovery rate	
$\mu_g$	death rate	